International Journal of Electrical Engineering, Mathematics and Computer Science

E-ISSN: 3048-1945
P-ISSN: 3048-1910

Research Article

Baseline Vapour Pressure Deficit Dynamics in an Emersed Anubias Cultivation Incubator: Sensor Construct Validity and Humidity-Governed VPD Drivers

Al Barra Harahap[1*], Vera Khoirunnisa[2], Aprilia Siregar[3], Sintya Shety Simanjuntak[4]

[1-4] Engineering Physics, Faculty of Industrial Technology, Institut Teknologi Sumatera; Indonesia
* Corresponding Author: albarra.harahap@tf.itera.ac.id

Abstract. Vapour pressure deficit (VPD) has gained recognition as a physiologically superior microclimate control variable in controlled-environment agriculture, yet no quantitative VPD characterisation exists for emersed cultivation of variegated Anubias barteri var. nana 'Pinto'. This study characterises the VPD microclimate of an ebb-and-flow cyber-physical incubator equipped with an MLX90614 infrared radiometric sensor, two calibrated DHT22 humidity sensors, a DS18B20 nutrient solution sensor, and an ESP32-S3 microcontroller. A 5.36-hour passive commissioning session yielded 1,884 valid data rows at a 10-second logging interval. The mean baseline VPD_{rad} was 0.703 ± 0.022 kPa, falling within the upper portion of the reference envelope inferred from available literature on emersed Anubias acclimatisation. Indoor relative humidity was identified as the dominant VPD driver ($r = -0.695$, $R^2 = 0.483$), while air temperature showed negligible association ($r = -0.008$), supporting mist actuation as the appropriate primary control strategy. The MLX90614 recorded a consistent radiometric offset of $\Delta T\_rad = -1.61 \pm 0.10$ °C relative to indoor air temperature, reflecting the composite FOV average of cooler evaporative surfaces; the resulting VPD_{rad} was 0.327 kPa (32%) lower than the air-temperature-only estimate, demonstrating that the choice of surface temperature reference has a material effect on the computed VPD. A persistent ambient VPD gradient of +0.540 kPa was documented throughout the session, quantifying the continuous moisture gradient from the incubator interior to the ambient environment. These results establish a quantitative VPD baseline for emersed Anubias cultivation, define the construct validity boundaries of the sensor suite, and provide the empirical foundation for a companion closed-loop Fuzzy-PI VPD controller.

Keywords: Anubias Barteri; Controlled-Environment Agriculture; Emersed Cultivation; Infrared Radiometric Temperature; Vapour Pressure Deficit.

Received : April 30, 2025

Revised : May 27, 2025

Accepted : June 22, 2025

Published : June 30, 2025

Current Ver.: June 30, 2025

1. Introduction

Controlled-environment agriculture (CEA) has emerged as a critical strategy for decoupling crop production from climatic variability, enabling year-round cultivation under precisely managed microclimate conditions (Chen et al., 2025; Shamshiri et al., 2018). Among the environmental parameters governing plant growth, vapour pressure deficit (VPD), defined as the difference between the saturation vapour pressure at a reference surface and the actual vapour pressure of the surrounding air, has gained recognition as a physiologically superior control variable compared to relative humidity (RH) alone. Unlike RH, VPD integrates both temperature and humidity into a single metric that directly quantifies the evaporative demand placed on plant tissue (López et al., 2021). Inoue et al. demonstrated that maintaining stable, low-VPD conditions in lettuce significantly improved stomatal conductance and photosynthetic rates compared to high-VPD and fluctuating-VPD environments, highlighting the direct link between VPD dynamics and crop performance in CEA settings (Inoue et al., 2021).

Despite this growing body of knowledge for temperate food crops, the application of VPD-based microclimate characterisation to high-value tropical ornamental aquatic plants cultivated under emersed conditions remains largely unexplored. Aquatic macrophytes in the family Araceae are physiologically capable of transitioning between submersed and emersed life forms, a flexibility mediated by abscisic acid (ABA) signalling and associated with distinct morphological and stomatal adaptations (Wanke, 2011). In the emersed state, these plants are directly exposed to atmospheric VPD, making their transpiration dynamics fundamentally different from their submerged counterparts and potentially sensitive to microclimate conditions in ways not yet characterised.

Anubias barteri var. nana 'Pinto' is a variegated cultivar of considerable commercial value in the ornamental aquatics industry, distinguished by sectors of partially achlorophyllous white leaf tissue. As a member of the Araceae, Anubias species are globally traded ornamental aquatic plants whose cultivation increasingly favours the emersed form for accelerated growth rates and propagation efficiency (Luo et al., 2025). The white tissue sectors of 'Pinto' present a biological vulnerability absent in fully chlorophyllous cultivars: lacking the photosynthetic capacity to drive active metabolic recovery, these sectors are hypothesised to be disproportionately susceptible to transpiration-driven calcium deficiency when stomatal conductance is suppressed by excessive VPD, a mechanism analogous to tipburn necrosis in lettuce under transpiration-limiting conditions of high humidity and inadequate air movement (Frantz et al., 2004). This hypothesis remains untested in Anubias 'Pinto' and constitutes a primary biological motivation for establishing quantitative VPD control in emersed cultivation systems. The present study therefore addresses an engineering prerequisite: establishing a quantitative microclimate baseline and validating the sensor suite before biological experiments can be meaningfully designed.

The ebb-and-flow subirrigation method has been established as an effective irrigation strategy for containerised plant production, offering advantages in water use efficiency, root zone control, and minimisation of foliar wetting compared to overhead irrigation methods (Jani et al., 2021; Wang et al., 2022). Applied to emersed ornamental aquatic plant cultivation, ebb-and-flow systems enable periodic flooding of the root zone while maintaining a well-defined aerial microclimate, a configuration well-suited to integrating closed-loop VPD control through mist and ventilation actuators. Hydroponic and subirrigation systems increasingly incorporate Internet-of-Things (IoT) sensor networks and cyber-physical control architectures to enable autonomous environmental regulation (Ayaz et al., 2019; Zamora-Izquierdo et al., 2019), and nutrient solution management in such systems is an active area of optimisation (Fathidarehnijeh et al., 2023). To our knowledge, published cyber-physical implementations for emersed ornamental aquatic plant cultivation with VPD as the primary controlled variable have not been reported in the literature.

A fundamental prerequisite for designing any closed-loop VPD control system is the availability of a reliable, characterised sensor suite and a quantitative baseline characterisation of the plant-environment microclimate under passive conditions. Low-cost capacitive humidity sensors such as the DHT22 have been validated for greenhouse humidity monitoring applications with acceptable accuracy (Wardani et al., 2023), while infrared radiometric sensors such as the MLX90614 offer a non-contact proxy for surface temperature. Their field-of-view integration characteristic means that in a mixed-surface environment of leaf, water, substrate, and chamber floor, the measured radiometric temperature (T_rad) represents a composite signal rather than a true single-leaf temperature (González Rivero et al., 2023). This construct validity constraint has significant implications for the interpretation of VPD computed from T_rad and must be explicitly addressed in any system claiming leaf-level VPD measurement. Prior work from this laboratory on cyber-physical environmental control systems (Harahap, Drantantiyas, et al., 2025; Harahap, Khoirunisa, et al., 2025) provides methodological context for the embedded sensing and control architecture adopted in the present study.

This study characterises the baseline VPD microclimate of an ebb-and-flow cyber-physical incubator designed for emersed Anubias barteri var. nana 'Pinto' cultivation and establishes the valid operating boundaries of the heterogeneous sensor suite, specifically the MLX90614 infrared radiometric sensor and DHT22 capacitive humidity sensors, used to measure and regulate it. A 5.36-hour passive commissioning session is reported, covering VPD baseline characterisation, dominant driver analysis, ambient-to-indoor VPD gradient quantification, and an explicit construct-validity assessment of the radiometric temperature proxy.

The main contributions of this study are as follows. To our knowledge, this work presents the first quantitative VPD baseline for an emersed Anubias cultivation incubator (VPD_rad = 0.703 ± 0.022 kPa, 5.36-hour passive session), providing a reference for future VPD-controlled cultivation studies in this species group. Indoor relative humidity is established as the primary VPD driver (r = −0.695) over air temperature (r = −0.008), directly informing actuator selection for subsequent closed-loop design. A construct-validity analysis of T_rad from the MLX90614 in a mixed-surface incubator FOV is provided, with a consistent offset of ΔT_rad = −1.61 ± 0.10 °C relative to ambient air temperature, establishing explicit validity boundaries for interpreting VPD_rad as a relative indicator rather than an absolute leaf-surface measurement. An ambient VPD gradient characterisation (VPD_amb = 1.243 kPa; ΔVPD = +0.54 kPa) quantifies the persistent moisture difference between the incubator interior and the laboratory environment, a disturbance input relevant to feed-forward control design in companion work.

2. Materials and Method

Incubator System Design

The experimental platform is a single-rack ebb-and-flow cyber-physical incubator purpose-built for emersed ornamental aquatic plant cultivation at an air-conditioned indoor laboratory. The physical structure consists of a transparent polycarbonate growth rack containing a subirrigation tray that is periodically flooded with nutrient solution via a submersible pump relay, then allowed to drain by gravity, a configuration that maintains root-zone moisture while exposing the aerial canopy to a controlled atmospheric microclimate (Jani et al., 2021; Wang et al., 2022). The test specimens were Anubias barteri var. nana 'Pinto' plants cultivated on the growth substrate within the rack under the emersed condition, with leaves fully exposed to the incubator air volume. The physical arrangement of sensors, actuators, and fluid circulation components is illustrated in Figure 1.

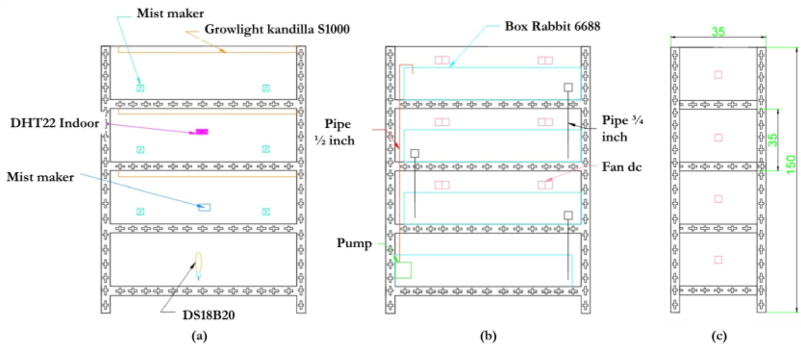

Figure 1. Schematic diagram of the ebb-and-flow incubator. (a) Rear view (b) Front view (c) Side view: rack dimensions (width 35 cm, shelf height 35 cm, total height 150 cm).

Sensor Suite and Calibration

The sensor suite integrates four measurement modalities targeting the variables required for VPD computation: surface radiometric temperature, ambient air temperature and humidity inside and outside the chamber, and nutrient solution temperature. Table 1 summarises the sensor specifications, calibration status, and firmware interface assignments.

Table 1. Sensor suite specifications.

Sensor	Measured Parameter	Interface	Nominal Accuracy	Calibration Applied
MLX90614	T_{rad} (radiometric surface temperature)	I2C, address 0x5A	±0.5 °C (object, black-body condition)	None, raw radiometric value
DHT22 (indoor)	T_{indoor}, RH_{indoor}	Single-wire, GPIO 16	±0.5 °C / ±2–5% RH	Linear correction: y = a + bx
DHT22 (outdoor)	$T_{outdoor}$, $RH_{outdoor}$	Single-wire, GPIO 17	±0.5 °C / ±2–5% RH	Linear correction: y = a + bx
DS18B20	T_{water} (nutrient solution)	1-Wire, GPIO 4	±0.5 °C	Linear correction: y = a + bx

The MLX90614 infrared radiometric thermometer (Melexis, Belgium) measures the apparent radiometric temperature of all surfaces within its 90° half-angle field of view (FOV) via a thermopile detector responding to long-wave infrared emission (8–14 μm). In the incubator geometry, the sensor was positioned above the plant canopy at an approximate height of 8 cm above the uppermost leaf surface, yielding an estimated FOV footprint of approximately 201 cm^2 at canopy level such that its FOV encompassed leaf surfaces, wet growth substrate, and portions of the ebb-and-flow tray floor. The MLX90614 was operated without empirical calibration against a reference in this study. While the manufacturer specifies an object temperature accuracy of ±0.5 °C under standardised blackbody conditions, this specification does not account for the emissivity heterogeneity of the mixed-surface FOV. A calibration against a contact thermocouple on representative leaf tissue is recommended before making absolute leaf-surface temperature claims and is deferred to future work. In the present characterisation, T_rad is therefore treated as a relative radiometric proxy, and VPD_rad derived from it is interpreted as a relative VPD indicator rather than a calibrated leaf-surface VPD.

The DS18B20 one-wire digital thermistor (Maxim Integrated, USA) was submerged in the nutrient solution reservoir to monitor water temperature, which contributes to the radiometric average received by the MLX90614 during flood cycles. Both DHT22 capacitive humidity and temperature sensors (AOSONG Electronics, China) are low-cost sensors previously validated for greenhouse humidity monitoring applications (Wardani et al., 2023); the indoor unit was positioned within the incubator air volume at canopy height, and the outdoor unit was positioned in the ambient laboratory environment to characterise the external VPD boundary condition.

All sensors except the MLX90614 were calibrated against reference instruments prior to data collection using simultaneous side-by-side comparison over a range of naturally occurring temperature and humidity conditions. Correction functions were fitted as first-order linear equations of the form y = a + bx, where x is the raw sensor output and y is the calibrated value. The resulting coefficients are listed in Table 2.

Table 2. Sensor calibration coefficients (y = a + bx).

Sensor	Parameter	Offset a	Slope b	R^2
DHT22 indoor	Temperature (°C)	−0.076	1.002	0.99997
DHT22 indoor	Relative humidity (%)	−2.601	0.876	0.99999
DHT22 outdoor	Temperature (°C)	−0.046	1.001	0.99118
DHT22 outdoor	Relative humidity (%)	+4.418	0.824	0.98246
DS18B20	Temperature (°C)	−0.249	1.010	0.99843
MLX90614	—	Not calibrated	Not calibrated	Not calibrated

Input signals from the DHT22 sensors were smoothed using a moving-average filter prior to VPD computation: a window of N = 5 samples for the indoor unit and N = 3 samples for the outdoor unit, implemented in firmware as a circular buffer with NaN-exclusion. The DS18B20 was read in non-blocking mode with a 12-bit conversion resolution (conversion time ≤ 750 ms) and was not smoothed, as one-wire digital thermistors exhibit an inherently lower noise floor than capacitive sensors. Sensor health monitoring was implemented in firmware: consecutive NaN readings from either DHT22 unit reaching a threshold of five cycles triggered a warning message prepended with '#' in the serial log, preserving the integrity of the CSV data stream.

VPD Computation

Two VPD quantities were computed in this study, reflecting the two physically distinct reference conditions available from the sensor suite. Both are based on the Tetens approximation for saturation vapour pressure:

$$e_s(T) = 0.6108\, e^{(17.27T/(T+237.3))} [\text{kPa}] \quad (1)$$

where T is temperature in degrees Celsius. This formulation is the standard Magnus-type equation widely used in agricultural meteorology and plant physiology (Inoue et al., 2021; López et al., 2021).

The primary computed quantity, designated VPD_rad, uses the radiometric temperature T_rad from the MLX90614 as a proxy for the surface temperature of the plant canopy, and the indoor air vapour pressure from the calibrated DHT22 indoor sensor as the ambient reference:

$$VPD_{rad} = e_s(T_{rad}) - e_s(T_{indoor}) \cdot (RH_{indoor}/100) [\text{kPa}] \quad (2)$$

This formulation is a modified leaf-level VPD equation in which T_{rad} replaces T_{leaf}. As noted in Section 2.2, T_{rad} is a composite radiometric average across the sensor FOV and not a single-leaf measurement, which introduces a systematic offset between VPD_{rad} and a true leaf-surface VPD. The consistent ΔT_{rad} offset ($T_{rad} - T_{indoor}$) observed in the commissioning data reflects this composite character and is analysed in Section 3.3.

The ambient VPD, designated VPD_amb, characterises the external boundary condition and is computed from the calibrated outdoor DHT22 readings:

$$VPD_{amb} = e_s(T_{outdoor}) \cdot (1 - RH_{outdoor}/100) [\text{kPa}] \quad (3)$$

VPD_{amb} does not involve a surface temperature term because it represents the moisture deficit of the free atmospheric air outside the incubator rather than a plant-atmosphere gradient. The difference $\Delta VPD = VPD_{amb} - VPD_{rad}$ is reported alongside the primary VPD_rad characterisation to quantify the persistent moisture gradient between the incubator interior and the ambient laboratory environment.

All VPD computations were performed in real-time on the ESP32-S3 microcontroller at each 10-second logging cycle, with results written directly to the serial data stream in CSV format.

Data Logging and Acquisition

Data were logged at a fixed interval of 10 seconds throughout the commissioning session. At each logging cycle, the firmware assembled a single CSV row containing 18 columns: Timestamp (DD/MM/YYYY HH:MM:SS from the DS3231 RTC), T_indoor, RH_indoor, T_rad, ΔT_rad, T_outdoor, RH_outdoor, T_water, VPD_rad, VPD_amb, dVPD/dt (first-order finite difference of VPD_rad), Fan_%, Mist_%, Mode, Pump, Lamp, Zone, and t_since_pump_s (elapsed time in seconds since the last pump relay event). Rows beginning with '#' are comment lines (warnings, status messages, header re-emissions) and are excluded from numerical analysis.

The serial data stream was captured at 115,200 baud via USB using a PC terminal, then exported to a CSV file for offline processing. Post-collection, data were imported into Python (version 3.12) using the pandas library (version 2.2) for statistical analysis and visualisation. Rows containing NaN values in T_indoor or RH_indoor were excluded from statistical computations but retained in the full dataset with explicit NaN notation, consistent with data integrity practices for sensor characterisation studies (González Rivero et al., 2023).

Commissioning Experimental Protocol

The commissioning session was conducted in an air-conditioned indoor laboratory at ITERA. The session ran from 10:31 to 15:52 local time (UTC+7), totalling 5 hours and 21 minutes (5.36 hours). The 5.36-hour window was selected to capture a complete midday thermal cycle under stable air-conditioning, consistent with the commissioning objective of characterising passive equilibrium dynamics prior to closed-loop deployment. Logging commenced immediately upon firmware initialisation following hardware bring-up; sensor readings were available from the first logging cycle without a dedicated preflight hold.

The session was designed as a passive characterisation protocol. The fan actuator was operated at 100% duty cycle throughout to provide consistent forced convection and prevent boundary-layer stagnation at sensor and leaf surfaces. The mist actuator was held at 0% duty cycle. The LED grow lamp SSR was ON continuously to maintain photosynthetically active radiation consistent with normal cultivation conditions. The ebb-and-flow pump relay was maintained in the OFF state throughout the session to eliminate irrigation-cycle disturbances from the thermal and humidity baseline; the column t_since_pump_s confirmed that no pump event occurred during the 5.36-hour session. This configuration represents the passive dynamic equilibrium of the incubator under forced ventilation and constitutes the baseline against which future actuated VPD control performance will be benchmarked. The ambient laboratory environment ($T_{outdoor}$, $RH_{outdoor}$) was monitored simultaneously via the outdoor DHT22 to characterise the external boundary condition throughout the session.

Statistical Analysis

All statistical analyses were performed in Python using NumPy (version 1.26) and pandas (version 2.2). Descriptive statistics (mean, standard deviation, minimum, maximum) were computed for all logged variables over the full valid session duration after exclusion of NaN rows. Pearson correlation coefficients between VPD_{rad} and five candidate predictor variables were computed to identify the dominant sources of VPD variability under passive conditions. Given the high temporal autocorrelation inherent in 10-second interval data, the correlation coefficients and R^2 values are reported as descriptive measures of association rather than as inferential statistics; significance testing is noted where applicable but is not used to rank driver importance. Time-series trends were examined by computing 30-minute interval means to characterise intra-session variation in VPD_rad across the 5.36-hour session. The ΔT_{rad} offset was characterised statistically to quantify the systematic radiometric bias of the MLX90614 in the mixed-surface FOV configuration.

3. Results and Discussion

Baseline VPD Characterisation

The commissioning session yielded 1,902 total logged rows over 5.36 hours. Of these, 18 rows contained NaN values in T_{indoor} and RH_{indoor} following a mid-session microcontroller reset at approximately 13:05 local time. These 18 rows follow a mid-session microcontroller reset detected at approximately 13:05 local time and reflect DHT22 warm-up latency after the reset rather than primary sensor failure. The remaining 1,884 rows (99.05%) constitute the valid analytical dataset, spanning the full session from 10:31 to 15:52 local time at a 10-second logging interval.

The mean baseline VPD_rad over the valid session was 0.703 ± 0.022 kPa (mean ± SD), with a minimum of 0.557 kPa and a maximum of 0.764 kPa. The total range of 0.207 kPa across 5.36 hours reflects a microclimate that remained relatively stable without active humidity control, sustained by continuous forced ventilation at fan 100% duty cycle. Air temperature was notably stable throughout (T_{indoor} = 27.18 ± 0.11 °C), while indoor relative humidity showed moderate variation (RH_{indoor} = 71.4 ± 0.74%), with the majority of VPD fluctuation attributable to humidity dynamics rather than thermal variation, as shown by the correlation analysis in Section 3.2.

The intra-session evolution of VPD_rad, summarised in 30-minute intervals in Table 3, shows a rise from 0.697 kPa in the first interval (10:30) to a peak of 0.728 kPa around 12:00–12:30, driven by a simultaneous decline in indoor RH from 72.2% to 70.3%. VPD_{rad} then declined gradually through the afternoon to around 0.683–0.690 kPa by 15:00, coinciding with a partial RH recovery to 71.7–71.8% and a slight drop in T_{indoor} from 27.40 °C to 27.09 °C. The elevated SD in the 13:00 interval (±0.022 kPa versus ±0.012–0.014 kPa in adjacent intervals) reflects the gap in valid data caused by the mid-session reset, which produced a step discontinuity in the time series rather than a genuine VPD excursion. The overall pattern, a morning rise and an afternoon gradual decline, is consistent with the thermal and humidity dynamics of an air-conditioned indoor laboratory subject to building-level thermal load variation over the course of the day. The full intra-session time series is shown in Figure 2.

Table 3. Intra-session variation of VPD_{rad} and key environmental parameters in 30-minute intervals.

Time interval	n (rows)	VPD_{rad} mean (kPa)	VPD_{rad} SD (kPa)	RH_{indoor} mean (%)	T_{indoor} mean (°C)	T_{rad} mean (°C)	VPD_{amb} mean (kPa)
10:30	178	0.697	0.014	72.2	27.40	25.84	1.214

11:00	180	0.718	0.012	71.4	27.30	25.73	1.242
11:30	180	0.724	0.014	70.9	27.24	25.62	1.254
12:00	180	0.728	0.013	70.5	27.18	25.51	1.259
12:30	180	0.728	0.012	70.3	27.15	25.46	1.268
13:00	160	0.701	0.022	71.0	27.14	25.44	1.264
13:30	180	0.691	0.015	71.6	27.11	25.49	1.246
14:00	180	0.683	0.012	72.0	27.12	25.53	1.226
14:30	180	0.686	0.012	71.9	27.14	25.53	1.233
15:00	180	0.688	0.012	71.7	27.13	25.50	1.238
15:30	106	0.690	0.012	71.8	27.09	25.49	1.228

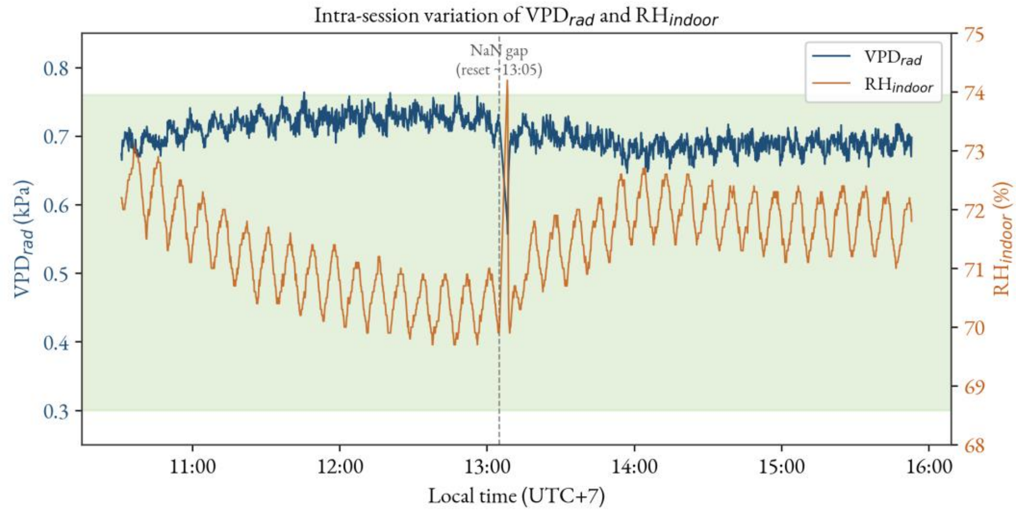

Figure 2. Intra-session variation of VPD_{rad} and RH_{indoor} under passive forced-ventilation conditions; the shaded band indicates the reference VPD envelope inferred from *(Rittirat et al., 2021)*.

VPD Drivers: Humidity Dominance over Temperature

Pearson correlation coefficients between VPD_rad and five candidate predictor variables were computed over the 1,884 valid data rows. The results are presented in Table 4.

Indoor relative humidity was the dominant predictor, with r = −0.695 and R^2 = 0.483, meaning RH variation alone accounts for approximately 48% of the observed VPD_{rad} variance under these passive conditions. Air temperature (T_{indoor}) showed no meaningful association with VPD_{rad} (r = −0.008), consistent with the exceptional thermal stability of the session (σ = 0.11 °C): across a 0.11 °C standard deviation in temperature, the corresponding change in es(T) is approximately 0.008 kPa, which is below the effective noise floor of the RH contribution. Under these conditions, VPD dynamics are humidity-governed rather than temperature-governed.

The radiometric temperature T_rad showed a weak positive association (r = +0.114, R^2 = 0.013). This is physically consistent: minor variations in the thermal state of the FOV composite cause small changes in es(T_{rad}), which propagate into VPD_{rad} independently of RH. The ΔT_{rad} term (r = +0.179) reflects the same physical interaction in difference form. The ambient VPD showed a modest positive association (r = +0.208, R^2 = 0.043), indicating that outdoor dryness variations do modestly propagate inward, though the low R^2 confirms that the enclosure provides substantial buffering from ambient fluctuations under forced ventilation.

Given the high temporal autocorrelation inherent in 10-second interval time-series data, the reported r and R^2 values are treated as descriptive measures of association. The effective degrees of freedom are substantially lower than n = 1,884, so the nominal p-values should not be used to rank driver importance; the magnitudes of r and R^2 serve that purpose.

Table 4. Pearson correlation coefficients between VPD_{rad} and candidate predictor variables

Variable	r	R^2	Note

RH_{indoor}	-0.695	0.483	Primary driver : humidity governs VPD under stable temperature
T_{indoor}	-0.008	0.000	Negligible : thermal variation (σ = 0.11 °C) too small to drive VPD
T_{rad}	+0.114	0.013	Weak positive : minor FOV composite thermal variation
ΔT_{rad}	+0.179	0.032	Modest : Reflects FOV composite thermal interaction with VPD computation

The dominance of RH over temperature as a VPD driver has a direct implication for closed-loop control design: the mist actuator, which directly raises indoor RH, is the appropriate primary actuator for VPD reduction. The fan actuator primarily influences boundary-layer air exchange rather than bulk temperature and is expected to have a secondary, condition-dependent effect on VPD. This inference from passive commissioning data will be examined against system identification results in companion work. VPD-based humidity control via mist actuation has been demonstrated in analogous CEA applications, including lettuce cultivation where RH-driven VPD fluctuations were the primary target of closed-loop intervention (Inoue et al., 2021), supporting the applicability of this driver structure to humidity-first control architectures more broadly.

Radiometric Temperature: Construct Validity Analysis

The MLX90614 recorded T_rad values consistently below T_indoor throughout the session, with a mean offset $\Delta T_{rad} = T_{rad} - T_{indoor} = -1.61 \pm 0.10$ °C (range: −2.20 to −1.38 °C). The low standard deviation of this offset over 5.36 hours indicates it is a systematic property of the measurement configuration rather than a transient physiological or environmental artefact.

The physical basis of this offset lies in the FOV geometry. The MLX90614 thermopile integrates thermal emission from all surfaces within its 90° half-angle FOV, which in the incubator encompasses Anubias leaf surfaces, wet growth substrate between petioles, and portions of the ebb-and-flow tray floor. All of these surfaces are wet or in evaporative contact with moisture and are therefore cooler than the surrounding air. The observed $\Delta T_{rad} \approx -1.61$ °C represents this composite radiometric average. It includes both genuine surface temperature depression due to evaporative cooling and any systematic sensor-level offset; these two components cannot be separated without a concurrent thermocouple measurement on representative leaf tissue, and this separation is deferred to future work. The intra-session variation of both temperatures and the persistent offset between them are shown in Figure 3. The choice of surface temperature reference has a material and quantifiable effect on the computed VPD, with a controller setpoint based on VPD_{rad} targeting a systematically lower moisture deficit than one based on VPD_{DHT} by 0.327 kPa at the observed operating conditions.

This distinction has a quantitative consequence for VPD computation. Using (T_{indoor}) as the surface reference instead of (T_{rad}), the RH-only formulation (VPD_{DHT}) that is applicable when no IR sensor is available, results in ($VPD_{DHT} = 1.031 \pm 0.027$) kPa, compared to ($VPD_{rad} = 0.703 \pm 0.022$) kPa. This represents a difference of (0.327) kPa, or approximately 32% of (VPD_{DHT}).

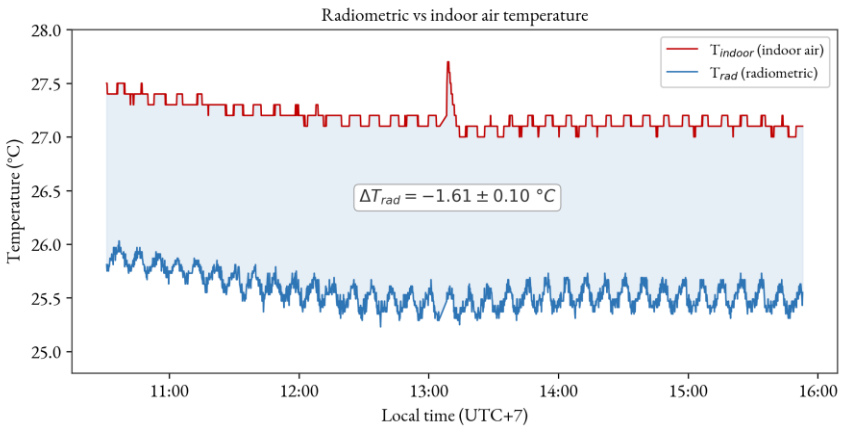

Figure 3. Intra-session variation of T_{rad} (MLX90614) and T_{indoor} (DHT22 indoor), showing a consistent negative offset of ΔT_rad = −1.61 ± 0.10 °C throughout the session.

Ambient VPD Gradient

The mean ambient VPD (VPD_amb) computed from the outdoor DHT22 was 1.243 ± 0.025 kPa throughout the session, ranging from 1.160 to 1.294 kPa. This is 1.77 times the mean indoor VPD_rad (0.703 kPa), reflecting considerably drier air in the ambient laboratory environment relative to the incubator interior.

The difference $(\Delta VPD = VPD_{amb} - VPD_{rad})$ was positive throughout the entire session, with a mean of +0.540 kPa (SD 0.029 kPa), a minimum of +0.455 kPa, and a maximum of +0.695 kPa. At no point during the 5.36-hour session did (ΔVPD) approach zero. This persistent positive gradient indicates that the incubator continuously loses moisture to the ambient environment even under forced ventilation with mist inactive. The magnitude of this gradient, which is comparable to the indoor (VPD_{rad}) itself, implies that sustained active mist intervention will be necessary to maintain any target indoor VPD below ambient over extended operation.

The weak coupling between VPD_amb and VPD_rad (r = +0.208, R^2 = 0.043) shows that ambient dryness variations propagate inward only partially, consistent with the polycarbonate enclosure and the wet substrate and tray surfaces providing meaningful buffering from outdoor fluctuations.

From a control engineering standpoint, the magnitude and persistence of ΔVPD quantify the steady-state disturbance load that a closed-loop VPD controller must continuously reject, providing the empirical basis for including VPD_amb as a feed-forward input in the companion controller design.

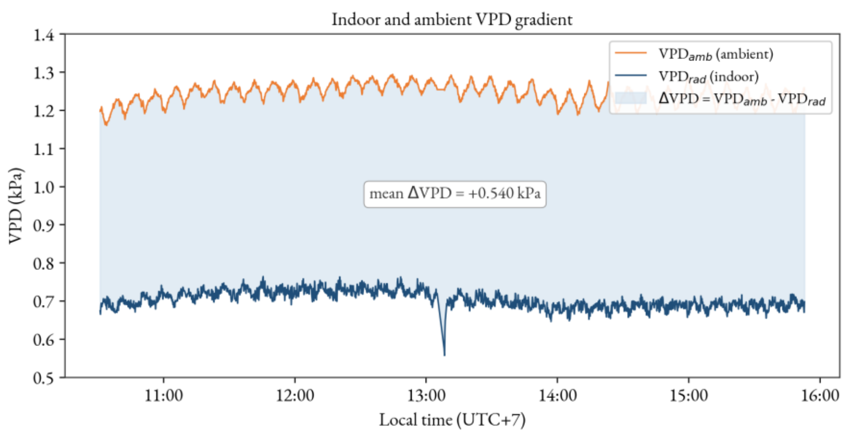

Figure 4. Intra-session variation of indoor VPD_{rad} and ambient VPD_{amb}, 10:31–15:52 local time. The shaded area represents $\Delta VPD = VPD_{amb} - VPD_{rad}$, which remained persistently positive throughout the session (mean +0.540 kPa, minimum +0.455 kPa).

Data Quality and Sensor Reliability

Of the 1,902 total logged rows, 18 rows (0.95%) contained NaN values in T_{indoor}, RH_{indoor}, and the derived VPD_{rad}. As described in Section 2.5, these rows follow a mid-session microcontroller reset detected at approximately 13:05 local time and reflect DHT22 warm-up latency after the reset rather than primary sensor failure. The firmware logged NaN values explicitly rather than propagating last-known readings, preserving data stream integrity. These 18 rows were excluded from all statistical analyses, yielding a valid dataset of 1,884 rows (99.05%).

The MLX90614 produced no indication of a frozen-value condition, defined as an extended sequence of identical readings, throughout the 5.36-hour session. T_{rad} showed gradual thermal variation consistent with the changing thermal state of the FOV composite surfaces, rather than the artificial flatness that would indicate I2C bus failure or sensor lock-up. The DS18B20 nutrient solution sensor produced stable readings throughout, consistent with the high thermal mass of the solution reservoir. No consecutive-failure warnings were generated by the DHT22 health monitoring beyond the post-reset warm-up period.

4. Conclusions

A 5.36-hour passive commissioning characterisation of an ebb-and-flow cyber-physical incubator for emersed Anubias barteri var. nana 'Pinto' cultivation yielded 1,884 valid data rows at a 10-second logging interval. The mean baseline VPD_rad was 0.703 ± 0.022 kPa with a total intra-session range of 0.207 kPa, placing it within the upper portion of the VPD range reported for emersed Anubias acclimatisation in the closest available reference, though that reference characterised a different species under different conditions and cannot serve as a species-specific target.

Indoor relative humidity was the dominant VPD driver ($r = -0.695$, $R^2 = 0.483$), while air temperature showed negligible association ($r = -0.008$) owing to the exceptional thermal stability of the chamber ($\sigma = 0.11$ °C). This asymmetric driver structure supports mist actuation as the primary control channel for subsequent closed-loop VPD regulation.

The MLX90614 recorded a consistent radiometric offset of $\Delta T_{rad} = -1.61 \pm 0.10$ °C relative to indoor air temperature throughout the session. The resulting VPD_{rad} was 0.327 kPa (32%) lower than the air-temperature-only estimate VPD_{DHT} (1.031 kPa), demonstrating that the choice of surface temperature reference has a material and quantifiable effect on the computed VPD, with direct consequences for setpoint interpretation in any closed-loop system built on this sensor suite. The fraction attributable to genuine surface cooling versus sensor-level bias cannot be resolved without thermocouple validation on representative leaf tissue, which is deferred to future work.

The ambient VPD gradient $\Delta VPD = VPD_{amb} - VPD_{rad}$ remained persistently positive throughout the session (mean +0.540 kPa, minimum +0.455 kPa), indicating continuous moisture loss from the incubator interior to the ambient environment and providing the empirical basis for incorporating VPD_amb as a feed-forward input in companion controller design.

The primary limitations of this study are the absence of thermocouple calibration for the MLX90614, meaning VPD_rad is a relative indicator rather than a calibrated leaf-surface VPD, and the untested status of the biological hypothesis linking VPD conditions to white-tissue damage in A. barteri var. nana 'Pinto'. Additionally, the characterisation is limited to a single 5.36-hour daytime session and does not capture nocturnal, multi-day, or seasonally varying VPD dynamics; extended monitoring under both passive and active mist control is needed to establish a more complete operational baseline. Future work will address biological validation, canopy-level PPFD measurement, and closed-loop controller deployment following system identification of the mist and fan actuator channels.

References

Ayaz, M., Ammad-Uddin, M., Sharif, Z., Mansour, A., & Aggoune, E.-H. M. (2019). Internet-of-Things (IoT)-Based Smart Agriculture: Toward Making the Fields Talk. *IEEE Access*, *7*, 129551–129583. https://doi.org/10.1109/ACCESS.2019.2932609

Chen, S., Liu, A., Tang, F., Hou, P., Lu, Y., & Yuan, P. (2025). A Review of Environmental Control Strategies and Models for Modern Agricultural Greenhouses. *Sensors*, *25*(5), 1388. https://doi.org/10.3390/s25051388

Fathidarehnijeh, E., Nadeem, M., Thomas, R., Cheema, M., & Krishnapillai, M. (2023). Current perspective on nutrient solution management strategies to improve the nutrient and water use efficiency in hydroponic systems. *Canadian Journal of Plant Science*, *104*(2), 88–102. https://doi.org/10.1139/cjps-2023-0034

Frantz, J. M., Ritchie, G., Cometti, N. N., Robinson, J., & Bugbee, B. (2004). Exploring the Limits of Crop Productivity: Beyond the Limits of Tipburn in Lettuce. *Journal of the American Society for Horticultural Science*, *129*(3), 331–338. https://doi.org/10.21273/JASHS.129.3.331

González Rivero, R. A., Morera Hernández, L. E., Schalm, O., Hernández Rodríguez, E., Alejo Sánchez, D., Morales Pérez, M. C., Nuñez Caraballo, V., Jacobs, W., & Martinez Laguardia, A. (2023). A Low-Cost Calibration Method for Temperature, Relative Humidity, and Carbon Dioxide Sensors Used in Air Quality Monitoring Systems. *Atmosphere*, *14*(2), 191. https://doi.org/10.3390/atmos14020191

Harahap, A. B., Drantantiyas, N. D. G., & Sasmita, I. A. (2025). Perancangan Sistem Deteksi Peta Panas (Heatmap) Keramaian Pengunjung di Area Publik Selama Pandemi COVID-19 Berbasis YOLOV4-Tiny. *Department of Electrical Engineering, Faculty of Engineering, Universitas Lampung*, *Vol. 19 No. 3 (2025).* https://doi.org/10.23960/elc.v19n3.2796

Harahap, A. B., Khoirunisa, V., Hutahaean, B. C., Tarigan, D. M., Siregar, S. I. G., & Harahap, H. P. (2025). Intelligent Comfort Management in Classrooms Using SSD-Based Occupant Detection and PMV-Guided Environmental Control. *Jurnal Otomasi Kontrol Dan Instrumentasi*, *17*(2), 147–161. https://doi.org/10.5614/joki.2025.17.2.9

Inoue, T., Sunaga, M., Ito, M., Yuchen, Q., Matsushima, Y., Sakoda, K., & Yamori, W. (2021). Minimizing VPD Fluctuations Maintains Higher Stomatal Conductance and Photosynthesis, Resulting in Improvement of Plant Growth in Lettuce. *Frontiers in Plant Science*, *12*, 646144. https://doi.org/10.3389/fpls.2021.646144

Jani, A. D., Meadows, T. D., Eckman, M. A., & Ferrarezi, R. S. (2021). Automated ebb-and-flow subirrigation conserves water and enhances citrus liner growth compared to capillary mat and overhead irrigation methods. *Agricultural Water Management*, *246*, 106711. https://doi.org/10.1016/j.agwat.2020.106711

López, J., Way, D. A., & Sadok, W. (2021). Systemic effects of rising atmospheric vapor pressure deficit on plant physiology and productivity. *Global Change Biology*, *27*(9), 1704–1720. https://doi.org/10.1111/gcb.15548

Luo, Y., Wei, L., Liu, W., Chen, J., Zhang, J., Yang, Z., Huang, S., & Zhou, Y. (2025). Integrative Physiological, Metabolomic and Transcriptomic Analyses Uncover the Mechanisms Underlying Differential Responses of Two Anubias Genotypes to Low-Temperature Stress. *Biomolecules*, *15*(11), 1520. https://doi.org/10.3390/biom15111520

Rittirat, S., Thammasiri, K., & Klaocheed, S. (2021). In Vitro Rapid Multiplication of a Highly Valuable Ornamental Aquatic Plant Anubias Heterophylla. *Trends in Sciences*, *18*(19), 3–3. https://doi.org/10.48048/tis.2021.3

Shamshiri, R., Kalantari, F., Ting, K. C., Thorp, K. R., Hameed, I. A., Weltzien, C., Ahmad, D., & Shad, Z. M. (2018). Advances in greenhouse automation and controlled environment agriculture: A transition to plant factories and urban agriculture. *International Journal of Agricultural and Biological Engineering*, *11*(1), 1–22.

Wang, K., Ali, M. M., Pan, K., Su, S., Xu, J., & Chen, F. (2022). Ebb-and-Flow Subirrigation Improves Seedling Growth and Root Morphology of Tomato by Influencing Root-Softening Enzymes and Transcript Profiling of Related Genes. *Agronomy*, *12*(2), 494. https://doi.org/10.3390/agronomy12020494

Wanke, D. (2011). The ABA-mediated switch between submersed and emersed life-styles in aquatic macrophytes. *Journal of Plant Research*, *124*(4), 467–475. https://doi.org/10.1007/s10265-011-0434-x

Wardani, I. K., Ichniarsyah, A. N., Telaumbanua, M., Priyonggo, B., Fil'aini, R., Mufidah, Z., & Dewangga, D. A. (2023). The feasibility study: Accuracy and precision of DHT 22 in measuring the temperature and humidity in the greenhouse. *IOP Conference Series: Earth and Environmental Science*, *1230*(1), 012146. https://doi.org/10.1088/1755-1315/1230/1/012146

Zamora-Izquierdo, M. A., Santa, J., Martínez, J. A., Martínez, V., & Skarmeta, A. F. (2019). Smart farming IoT platform based on edge and cloud computing. *Biosystems Engineering, Intelligent Systems for Environmental Applications*, *177*, 4–17. https://doi.org/10.1016/j.biosystemseng.2018.10.014